Nonlinear Neuro-Adaptive Control for MPPT Applied to Photovoltaic Systems

Arnaud Flanclair Tchouani Njomo[1,2] · Lionel Leroy Sonfack[1,2] · Rostand Marc Douanla[1,2] · Godpromesse Kenne[2]

Abstract

This paper presents an intelligent control technique using a nonlinear neuro-adaptive method. This method is based on a nonlinear model describing the dynamics of the boost converter, the PV array and the load for maximum power point tracking (MPPT) under varying environmental conditions. The proposed approach consisted of a radial basis function-neuro observer for online estimation of unknown PV system parameters (i.e., irradiation and temperature) and an online trained neuronal controller that ensures a satisfactory MPPT, whatever be the position of the photovoltaic panel. The real-time implementation of the proposed controller is achieved using Arduino Mega board. The performance of the proposed MPPT method is analyzed under different operating conditions and compared to those provided by the P&O method. Simulation results using MATLAB/Simulink software coupled to experimental results demonstrate the feasibility and the robustness of the proposed controller.

Keywords MPPT · RBF-neuro observer · DC/DC converter · Nonlinear neuro-adaptive · Real-time implementation

1 Introduction

Renewable energy capacity has increased these last years due to its main objective to alleviate the problem of pollution caused by traditional energy source (Kenne et al. 2017). Solar energy has particularly captivated more attention in recent decades (Le Feuvre and Wieczorek 2011; Yin et al. 2015; Parra et al. 2015). The lowest environmental impact and the

significant presence of solar radiation on the earth make photovoltaic (PV) systems one of the most interesting solutions to electricity generation (Sajadian and Ahmadi 2017; Chen et al. 2016; Mills and Wiser 2013). Indeed, the electricity produced by photovoltaic cells is an unstable energy because it depends on diverse factors such as the temperature, the level of solar irradiation, shadow, dirt, spectral characteristics of sunlight, and so on. It is therefore important to operate the photovoltaic system at the point of maximum power in order to increase its efficiency. Accordingly, the MPPT controller is one of the viable solutions to improve the productivity of PV systems under variable weather conditions.

The literature contains several approaches for MPPT in photovoltaic systems. These techniques include Hill Climbing (HC) (Kamarzaman and Tan 2013; Liu et al. 2008), perturb and observe (P&O) (Femia et al. 2009, 2005; Rezaei and Asadi 2005), incremental conductance (IC) (Li and Wang 2009; Reisi et al. 2013; Rajabi and Hassan Hosseini 2019), fractional open-circuit voltage (Mutoh et al. 2002; Yuvarajan and Xuc 2003), fractional short-circuit current (Kobayashi et al. 2004; Bekker and Beukes 2004), neural network (Hiyama et al. 1995, fuzzy logic methods (Won et al. 1994), and genetic algorithms (Larbes et al. 2009). These methods differ in several aspects such as oscillation around

✉ Arnaud Flanclair Tchouani Njomo
  tchouani1@gmail.com

  Lionel Leroy Sonfack
  sonfackleroy@gmail.com

  Rostand Marc Douanla
  douanlarost@yahoo.fr

  Godpromesse Kenne
  godpromesse@gmail.com

1 Unité de Recherche de Matière Condensée ,d'Electronique et de Traitement de Signal (UR-MACETS), Département de Physique, Faculté des Sciences, Université de Dschang, B.P. 69, Dschang, Cameroon

2 Unité de Recherche d'Automatique et d'Informatique Appliquée (UR-AIA), Département de Génie Electrique IUT FOTSO Victor Bandjoun, Université de Dschang, B.P. 134 , Bandjoun, Cameroon

the MPP, required sensors, convergence speed, complexity, cost and correct tracking.

There are several advantages such as fast tracking, robust operation, nonlinear systems tolerant and on-line training. Therefore, various artificial neural network-based PV MPPT techniques have been elaborated (Cha et al. 1997; Singh et al. 2014).

Nevertheless, the number of sensors required to implement any MPPT technique affects the decision process since these sensors induce the major burden for the overall PV system cost (Giraud and Salameh 1999; Mathew and Selvakumar 2011; Veerachary et al. 2003; Bendib et al. 2014). The cost, in addition to the lack of robustness of irradiance/temperature sensors, is the main limit for the artificial neural network-based MPPT methods (Mathew and Selvakumar 2011; Baek et al. 2010; Ko et al. 2008; Al-Amoudi and Zhang 2000; Pachauri and Chauhan 2014), especially when a wide PV plant, involving several hundreds of PV panels, is considered.

In this work, an intelligent control technique based on adaptive neural network for maximum power point tracking during unexpected changes in atmospheric conditions is proposed. The idea is to evolve a sensorless controller that does not require climatic variable sensors (i.e., temperature and solar radiation) and to provide a satisfactory MPPT, whatever the position of the photovoltaic panel. Specifically, a sensorless nonlinear neuro-adaptive controller is designed using the RBF-neural network observer technique based on a nonlinear model describing the whole system, including the PV arrays, and the boost converter. The proposed adaptive controller involves online estimation of the model uncertain parameters that depend on radiation and temperature. Based on the obtained simulation results in Matlab/Simulink environment, the adaptive neuro-controller actually tracks effectively and efficiently the maximum power point. Additionally, experimental implementation using an Arduino Mega board is carried out.

The remainder of the work is organized as follows: Sect. 2 presents in detail the elements of a PV conversion system. In Sect. 3, the proposed approach is introduced, and the stability is investigated. Sections 4 and 5 present, respectively, the simulation and experimental results. The conclusions are given in Sect. 6.

2 PV System Model

Figure 1 shows the basic structure of a photovoltaic system. It consists of a DC/DC converter, a photovoltaic generator, a load and the proposed MPPT control unit. The main function of the converter is to interface the output of the photovoltaic generator to the load and to track the MPP.
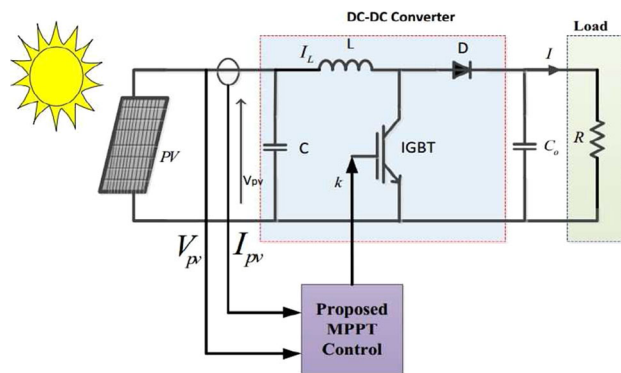
Fig. 1 Photovoltaic system made up of a PV array, a DC/DC converter and the proposed MPPT control algorithm
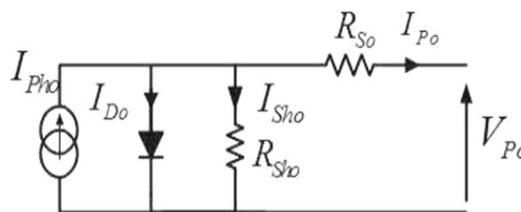

Fig. 2 Electrical model of a photovoltaic cell

Photovoltaics is the direct conversion of light into electrical energy. Figure 2 shows the equivalent circuit of a photovoltaic cell (Rekioua and Matagne 2012; Safari and Mekhilef 2011; Moura and Chang 2013; Tan et al. 2010). In the PV system control literature, this circuit has been considered as a sufficiently good representation of the physical system for the purposes of MPPT control design (Masters 2004; Vachtsevanos and Kalaitzakis 1987; Villalva et al. 2009; Kwon et al. 2008; Tchouani Njomo et al. 2020). The solar cell terminal current is expressed as follows:

$$I_{Po} = I_{Pho} - I_{Do} - I_{Sho} \tag{1}$$

where I_{Pho} is the photocurrent (current generated by radiation), I_{Do} is the current through the diode, and I_{Sho} is the current through the parallel resistor.

The relationship between the current I_{Pho} and the voltage V_{Po} of equivalent circuit of the photovoltaic cell is given by:

$$I_{Po} = I_{Pho} - I_{so}\left[\exp\left(\frac{V_{Po} + I_{Po}R_{so}}{nV_T}\right) - 1\right] - \frac{V_{Po} + I_{Po}R_{so}}{R_{Sho}} \tag{2}$$

The relation between the current I_{Po} and the voltage V_{Po} in the ideal conditions ($R_{so} = 0$, $R_{Sho} = \infty$) is described by the following equation:

$$I_{Po} = I_{Pho} - I_{so}[\exp(BV_{Po}) - 1] \tag{3}$$

$$B = \frac{q}{nKT} \tag{4}$$

where I_{so} is the cell reverse saturation current; K is the Boltzmann's constant; T is the cell temperature, and q is the electron charge. The generated photocurrent I_{Pho} is given by the following equation:

$$I_{Pho} = [I_{SCR} + K_I (T - T_{or})] \frac{G}{1000} \tag{5}$$

The cell saturation current I_{so} can be shown as:

$$I_{so} = I_{sor} \left[\frac{T}{T_{or}} \right]^3 \exp \left[\frac{EG}{nK} \left(\frac{1}{T_{or}} - \frac{1}{T} \right) \right] \tag{6}$$

where I_{SCR} is the short circuit current at 298.15 K and 1000 W/m², T_{or} is the reference temperature, G is the solar radiation, EG is the bandgap energy of the semiconductor, and I_{sor} is the nominal saturation current. A photovoltaic generator is composed of elementary photovoltaic cells connected in series-parallel manner in order to obtain the desired electronic characteristics such as power, short-circuit current or open-circuit voltage. This photovoltaic generator exhibits a nonlinear V_{PV}–I_{PV} characteristics given, approximately and ideally, by the following equation:

$$I_{PV} = I_{php} - I_{sp}[\exp(A_{pv}V_{PV}) - 1] \tag{7}$$

where I_{PV} and V_{PV} are, respectively, the current and voltage of photovoltaic generator. $I_{sp} = N_p I_{so}$ is the saturation current of the photovoltaic generator, $I_{php} = N_p I_{Pho}$ is the photocurrent of the photovoltaic generator, and $A_{pv} = B/N_s$ is photovoltaic generator constant. N_s is the number of PV connected in series, and N_p is the number of parallel parts.

The specifications of the PV module used in this paper are given in Table 1. The corresponding power value $P_{mp} = V_{mp} I_{mp}$ is called MPP. The typical $I_{PV} - V_{PV}$ and $P_{PV} - V_{PV}$ characteristics of the MSX60 PV module are shown in Fig. 3. It can be seen from this figure that an increase in irradiance results in a power increment. However, an increase in PV temperature causes power decrement.

A DC/DC boost converter (Fig. 4) increases the PV voltage and provides a control actuator for MPPT. At the boost converter's output, a capacitor maintains a roughly constant voltage (Krein et al. 1990).

Applying Kirchhoff's laws to the circuit of Fig. 4, one obtains the following dynamic model:

$$\frac{di_L}{dt} = -(1 - k)\frac{Ri_L}{L} + \frac{1}{L}V_{PV} \tag{8}$$

$$\frac{dV_{PV}}{dt} = -\frac{1}{C}i_L + \frac{1}{C}I_{PV} \tag{9}$$

Table 1 Electrical characteristics of the MSX-60 photovoltaic

Description	MSX-60
Maximum power (Pmp)	60 W
Maximum power point voltage (Vmp)	17.1 V
Maximum power point current, (Imp)	3.5 A
Open-circuit voltage (Voc)	21.1 V
Short-circuit current (Isc)	3.8 A
The number of cells (NS)	36
Current/temp. coefficient (Ki)	0.003%/°C
Voltage/temp. coefficient (Kv)	− 0.08 V/°C
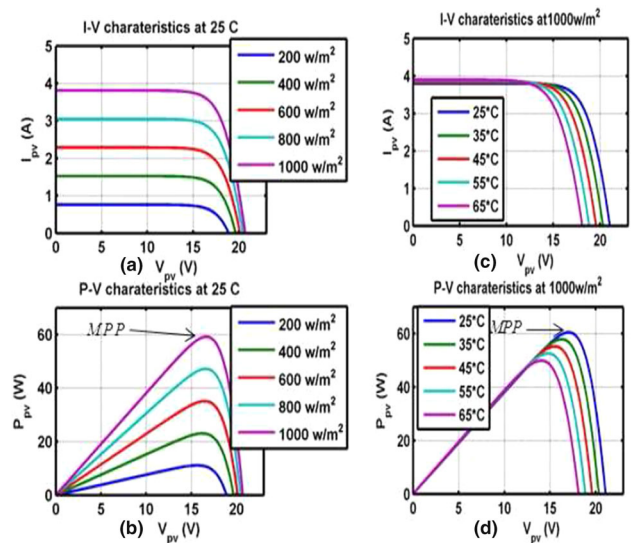
Fig. 3 Case of constant temperature and variable irradiation [current–voltage (**a**) and power–voltage characteristics (**b**)] and case of constant irradiation and variable temperature [current–voltage (**c**) and power–voltage characteristics (**d**)]
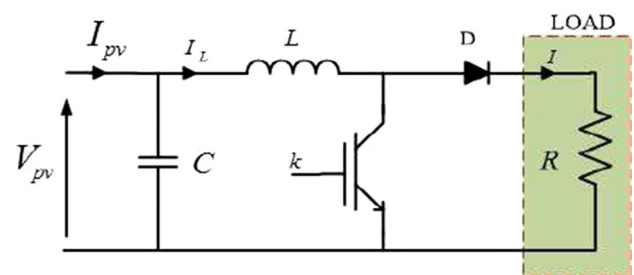
Fig. 4 Circuit diagram of DC/DC boost converter model

where i_L denotes the inductor current, V_{PV} the PV voltage, I_{PV} the pv current, and k the duty ratio. For the control design purpose, it is more convenient to consider the following averaged model:

$$\frac{dy_1}{dt} = -(1 - k)\frac{Ry_1}{L} + \frac{1}{L}y_2 \tag{10}$$

$$\frac{dy_2}{dt} = -\frac{1}{C}y_1 + \frac{1}{C}I_{PV} \tag{11}$$

where y_1 and y_2 denote the averaged value, respectively, of the current i_L, and the input voltage V_{PV}. The duty ratio k is the average value of the binary control k.

3 Design of Adaptive Controller for PV System

Combining (7) and (11) yields:

$$\frac{dy_2}{dt} = -\frac{1}{C}y_1 + \frac{1}{C}\rho_1(T,G) - \frac{1}{C}\varphi(T,V_{PV})\rho_2(T) \tag{12}$$

$$\rho_1(T,G) = I_{php} \tag{13}$$

$$\rho_2(T) = I_{sp} \tag{14}$$

$$\varphi(T,V_{PV}) = \exp\left(A_{pv}(T)V_{PV}\right) - 1. \tag{15}$$

The parameters ρ_2 depends only on the temperature, while ρ_1 depends on temperature T and irradiation G. The function φ depends on T. Because of the slowly fluctuating temperature, the effect of variation of φ is very small compared to the effect of ρ_1 and ρ_2. Therefore, the following approximation can be made:

$$\varphi(T,V_{PV}) \approx \exp\left[A_{pv}(T_{or})V_{PV}\right] - 1 \doteq \varphi(V_{PV}) \tag{16}$$

where T_{or} is a constant reference temperature. Combining (10), (12) and (15), we obtain the following average model of the PV system:

$$\dot{y}_1 = -(1-k)\frac{Ry_1}{L} + \frac{1}{L}y_2 \tag{17}$$

$$\dot{y}_2 = -\frac{1}{C}y_1 + \frac{1}{C}\rho_1(T,G) - \frac{1}{C}\varphi(y_2)\rho_2(T) \tag{18}$$

Given that the energy produced by PV is heavily dependent on temperature and irradiation, it is absolutely essential that the sensors used to measure temperature and irradiation are reliable. Hence, to ensure maximum power point tracking (MPPT), the controller must enforce the voltage y_2 to track as possible the unknown voltage V_{max} which depends on both T and G given by the sensors. However, the periodic maintenance of the sensors can be very expensive. The price of the sensors increases with their precision. The proposed approach aims to reduce the cost of sensor maintenance (eliminate the temperature and irradiation sensors) and improve the MPPT technique. In fact, the MPP (V_{max}, P_{max}) is reached when $\frac{\partial P_{PV}}{\partial V_{PV}}\mid_{V_{PV}=V_{max}}$ with $P_{PV} = V_{PV}I_{PV}$.

The condition of a maximum power point can be described as

$$\frac{\partial P_{PV}}{\partial V_{PV}} = I_{PV} + V_{PV}\frac{\partial I_{PV}}{\partial V_{VP}} = 0 \tag{19}$$

It follows, using (7), (13) and (14), that

$$\rho_1 - \rho_2\left[(1 + V_{max}A_{PV}(T_r))\exp\left(A_{PV}(T_r)V_{max}\right) - 1\right] = 0 \tag{20}$$

If ρ_1 and ρ_2 are known, Eq. (19) will be used to generate the optimal value of V_{max}. In this approach, ρ_1 and ρ_2 depending of T and G are supposed not be accessible to measurement. So we can estimate $\hat{\rho}_1$ and $\hat{\rho}_2$ using Eq. (18) rewritten as:

$$\dot{y}_2 = -\frac{1}{C}y_1 + F(y_2,\rho_1,\rho_2,t) \tag{21}$$

with $F(y_2,\rho_1,\rho_2,t) = \frac{1}{C}\rho_1(T,G) - \frac{1}{C}\varphi(y_2)\rho_2(T)$. Hence, in Eq. (20), $\dot{y}_2$ is unknown (I_l available in measurement), and it is not possible to use immediately Eq. (20) to estimate the unknown ρ_1 and ρ_2.

By applied the approach of neuro-observer as in Ahmed-Ali et al. (2009), it will be possible to estimate $\hat{\rho}_1$ and $\hat{\rho}_2$, and get V_{max}.

3.1 Design RBF-Neuro Observer

The application of the Taylor formula to Eq. (21) gives

$$\dot{V}_{PV} = -\frac{1}{C}I_l + f(y,\rho_1,\rho_2,t) + \Delta f(V_{PV},\rho_1,\rho_2,t) \tag{22}$$

where the term $f(V_{PV},\rho_1,\rho_2,t)$ can be approximated by RBF-NN and Eq. (21) becomes

$$\begin{aligned}\dot{\hat{V}}_{PV} &= -\frac{1}{C}\hat{I}_l + \Upsilon\left(\chi_{V_{PV}},\omega^*\right) + e_f\left(\chi_{V_{PV}}\right) + \Delta f\left(V_{PV},\rho_1,\rho_2,t\right)\\ &= -\frac{1}{C}\hat{I}_l + \sum\omega_j^*\phi\left(\|\chi_{V_{PV}} - C_j\|,v_j\right)\\ &\quad + e_f(\chi_{PV}) + \Delta f(V_{PV},\rho_1,\rho_2,t)\end{aligned} \tag{23}$$

with $\chi_{V_{PV}}^T = (V_{PV},I_l)$ the input vector or RBF neural network. In the assumption that $e_f(\chi_{V_{PV}})$ and the time-varying $\Delta f(V_{PV},\rho_1,\rho_2,t)$ are unknown and bounded by unknown positive value as $\mid e_f(\chi_{V_{PV}}) + \Delta h(V_{PV},\rho_1,\rho_2,t)\mid \leq \zeta(t)$, we rewrite Eq. (23) as:

$$\dot{\hat{V}}_{PV} = -\frac{1}{C}\hat{I}_l + \Upsilon\left(\chi_{V_{PV}},\hat{\omega}\right) + p\left(V_{PV},\hat{V_{PV}},t\right) \tag{24}$$

where the sliding robust terms $p(V_{PV},\hat{V_{PV}},t) = -\hat{\zeta}(t)\text{sgn}(e_2)$ are introduced to compensate the effect of the uncertainty

$\Delta f(V_{\mathrm{PV}}, \rho_1, \rho_2, t)$ which cannot be approximated by a static neural network.

By taking errors as $e_1 = \hat{I}_l - I_l$, $e_2 = \hat{V}_{\mathrm{PV}} - V_{\mathrm{PV}}$ deriving e_2 with respect to time, we obtain

$$
\begin{aligned}
\dot{e}_2 &= \dot{\hat{V}}_{\mathrm{PV}} - \dot{V}_{\mathrm{PV}} \\
&= -\frac{1}{C} e_1 + \sum \hat{\omega}_j \phi \left(\parallel \chi_{V_{\mathrm{PV}}} - C_j \parallel, \nu_j \right) \\
&\quad - \sum \omega_j^* \phi \left(\parallel \chi_{V_{\mathrm{PV}}} - C_j \parallel, \nu_j \right) + \zeta \left(V_{\mathrm{PV}}, \hat{V_{\mathrm{PV}}}, t \right) \\
&\quad - e_f(\chi) - \Delta f (V_{\mathrm{PV}}, \rho_1, \rho_2, t)
\end{aligned} \tag{25}
$$

By using Taylor series expansion, Eq. (25) becomes

$$
\begin{aligned}
\dot{e}_2 &= -\frac{1}{C} e_1 + \sum (\hat{\omega}_j - \omega_j^*) \frac{\partial \Upsilon}{\partial \omega} \mid_{\omega = \hat{\omega}} + \\
&\quad + \zeta(V_{\mathrm{PV}}, \hat{V_{\mathrm{PV}}}, t) - e_f(\chi_{V_{\mathrm{PV}}}) - \Delta f(V_{\mathrm{PV}}, \rho_1, \rho_2, t)
\end{aligned} \tag{26}
$$

The Lyapunov candidate function is considered as follows:

$$
\Pi = \frac{1}{2} e_2^2 + \frac{1}{2} \sum \left(\hat{\omega}_j - \omega_j^* \right)^2 \tag{27}
$$

Hence,

$$
\begin{aligned}
\dot{\Pi} &= e_2 \dot{e}_2 + \sum \dot{\hat{\omega}}_j \left(\hat{\omega}_j - \omega_j^* \right) \\
&= -\frac{1}{C} e_1 e_2 + \zeta \left(V_{\mathrm{PV}}, \hat{V_{\mathrm{PV}}}, t \right) - e_2 \big(e_f(\chi_{V_{\mathrm{PV}}}) \\
&\quad + \Delta f \left(V_{\mathrm{PV}}, \rho_1, \rho_2, t \right) \big) \\
&\quad + \sum \left(\hat{\omega}_j - \omega_j^* \right) \left[\dot{\hat{\omega}}_j + e_2 \frac{\partial \Upsilon}{\partial \omega_j} \mid_{\omega = \hat{\omega}} \right]
\end{aligned} \tag{28}
$$

By choosing

$$
p(V_{\mathrm{PV}}, \hat{V_{\mathrm{PV}}}, t) = -\dot{\hat{\zeta}}(t) \mathrm{sgn}(e_2) \tag{29}
$$

$$
\begin{aligned}
\dot{\hat{\omega}}_j &= \mathrm{Proj} \left[-e_2 \frac{\partial \Upsilon}{\partial \omega_j} \mid_{(\omega_j = \hat{\omega}_j)} \right], \quad j = 1, \dots, N \\
&= \begin{cases} -e_2 \frac{\partial \Upsilon}{\partial \omega_j} & \text{if } \mid \hat{\omega}_j \mid < R_\omega \\ 0 & \text{otherwise} \end{cases}
\end{aligned} \tag{30}
$$

$$
\dot{\hat{\zeta}}(t) = \begin{cases} \alpha_t & \text{if } e_2 \neq 0 \\ 0 & \text{if } e_2 = 0 \end{cases} \tag{31}
$$

with $\alpha(t) > 0$, $\hat{\zeta}(0) = 0$, and Proj(.) the well-known projection function on the compact set $\Omega_\omega = \{\omega : \parallel \omega \parallel \leq R_\omega\}$

$$
\dot{\Pi} \leq -\frac{1}{C} \mid e_1 e_2 \mid -\dot{\hat{\zeta}}(t) \mid e_2 \mid. \tag{32}
$$

Hence, the error e_2 will converge to the origin.

Remark 1 The width ν_j and the center C_j of the j-th hidden unit are chosen by clustering technique (Jain and Dubes

1988) as:

$$
\nu_{ij} = \frac{\ell_{i\,\max} - \ell_{i\,\min}}{N} \tag{33}
$$

$$
C_{ij} = \ell_{i\,\min} + \frac{2j - 1}{2} \nu_{ij} \tag{34}
$$

where $\ell_{i\,\min}$ and $\ell_{i\,\max}$ are the lower and upper bounds of the i-th element of the RBF input vector ℓ, respectively.

For the estimation of ρ_1 and ρ_2, Eq. (21) becomes

$$
\hat{Z} = \frac{\lambda}{P + \lambda} \left[\hat{\rho}^T(t) D(V_{\mathrm{PV}}) \right] \tag{35}
$$

with $D(V_{\mathrm{PV}}) = [\frac{1}{c}; -\frac{1}{c} \varphi(V_{\mathrm{PV}})]$, and $\rho(t) = [\hat{\rho}_1; \hat{\rho}_2]$, $\hat{Z} = \frac{\lambda}{P + \lambda} [\dot{V}_{\mathrm{PV}} + \frac{1}{C} \hat{I}_l]$.

Let us define $e_0 = \hat{Z} - Z$, $\tilde{\rho}(t) = \hat{\rho} - \rho(t)$. The output estimation error satisfies

$$
e_0 = \frac{\lambda}{P + \lambda} \left[\tilde{\rho}^T(t) D(V_{\mathrm{PV}}) \right] \tag{36}
$$

which implies that

$$
\dot{e}_0 = -\lambda e_0 + \lambda \tilde{\rho}^T(t) D(V_{\mathrm{PV}}). \tag{37}
$$

To apply the Lyapunov synthesis method, we select the Lyapunov function as

$$
\Pi_1 = \frac{1}{2} e_0^2 + \frac{1}{2} \tilde{\rho}^T \Gamma^{-1} \tilde{\rho} \tag{38}
$$

where $\Gamma = \gamma I$ is a positive definite symmetric matrix that will ultimately appear in the adaptive law for updating $\hat{\rho}(t)$ as the learning rate or adaptive gain.

Computing the derivative of Π_1 yields:

$$
\begin{aligned}
\dot{\Pi}_1 &= e_0 \dot{e}_0 + \tilde{\rho}^T \Gamma^{-1} \dot{\hat{\rho}} \\
&= -\lambda e_0^2 + \lambda e_0 \tilde{\rho}^T(t) D(V_{\mathrm{PV}}) + \tilde{\rho}^T \Gamma^{-1} \dot{\hat{\rho}} \\
&= -\lambda e_0^2 + \tilde{\rho}^T(t) [\Gamma^{-1} \dot{\hat{\rho}} + \lambda e_0 D(V_{\mathrm{PV}})]
\end{aligned} \tag{39}
$$

By choosing

$$
\dot{\hat{\rho}}(t) = \mathrm{proj}[-\lambda \Gamma D(V_{\mathrm{PV}}) e_0] \tag{40}
$$

Equation (39) becomes

$$
\dot{\Pi}_1 = -\lambda e_0^2 < 0 \tag{41}
$$

From $\dot{\Pi}_1 < 0$, one concludes from the Lyapunov stability theory that $\hat{\rho}(t)$ remains uniformly bounded, and $\tilde{\rho}(t)$ converges to zero in finite time according to Barbalat's lemma (Slotin and Li 1991)
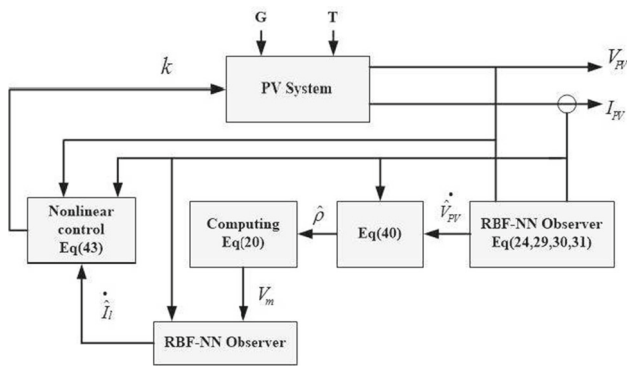
Fig. 5 Block diagram of the nonlinear neuro-adaptive MPPT control technique for PV systems

3.2 Controller Synthesis by Dynamic Inversion with Model Estimation

Recall that the control objective is to enforce the voltage V_{PV} to track the optimal point V_{max}, despite the system parameter uncertainties. To this end, the controller design is performed using Eq. (20) rewritten in from Eq. (42)

$$\dot{I}_l = H_{I_l} + Z_{I_l} k \tag{42}$$

where the functions $H_{I_l} = -\frac{R}{L} I_l + \frac{1}{L} V_{PV}$ and $Z_{I_l} = \frac{R}{L} I_l$ are both smooth functions available; k is the input control. We observed that in Eq. (42) the derivative state $\dot{I}_l$ is not available. For this reason, the RBF neuro-observer use in Sect. 3.1 will also be applied to get this derivative state $\hat{\dot{I}}_l$. Hence, the control law is given by:

$$k = \frac{1}{Z_{I_l}} [\hat{\dot{I}}_l - H_{I_l}] \tag{43}$$

The block diagram of the proposed nonlinear adaptive MPPT control technique for PV systems is depicted in Fig. 5.

4 Simulation Results

To demonstrate the efficiency of the proposed approach, different simulations are performed in Matlab/Simulink environment. The DC/DC converter is fed with a MSX-60 (60 W) solar panel from Solarex. The boost converter parameters are $C = 100\,\mu F$ and $L = 0.1\,\mu H$. A nominal value $R = 4.9\,\Omega$ is considered for the resistive DC load. The diode of the boost converter has a snubber resistance of 500 Ω, an internal resistance of 0.001 Ω and a forward voltage of 0.8 V. Internal and snubber resistances of the insulated-gate bipolar transistor(IGBT), used as the electronic switch of the boost converter are, 0.001 Ω and 0.1 MΩ, respectively. The switch-
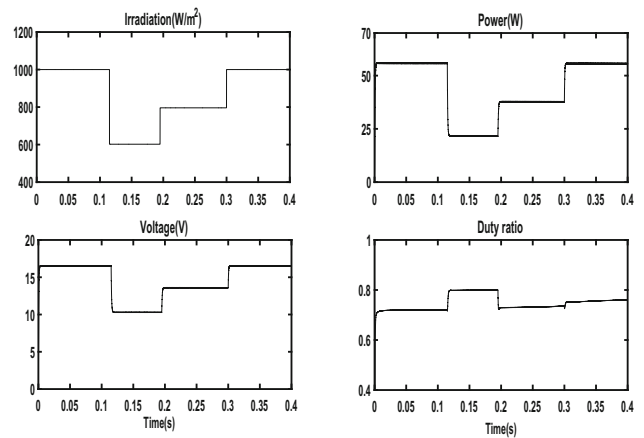

Fig. 6 The proposed MPPT controller during the irradiation change

ing frequency is set to $50\,kH_z$. The control design parameters are: $\gamma_1 = 1e-3$, $\gamma_2 = 0.1e-5$, $\lambda = 1\,rad/s$.

First, the system performances are assessed under two different operating conditions: the tracking under abrupt change in irradiation and the tracking under abrupt change temperature condition.

(a) System response to fast changing irradiation. During this test, a sun irradiation profile comprising various step changes is applied to the system, while a constant temperature of 25 °C is maintained. It is observed in Fig. 6 that the controller senses and follows the changes by extracting the maximum power corresponding to the given sun condition. The captured PV power in this condition varies between 21,5 W and 56 W. These values correspond (see Fig. 3) to the maximum points on the curves associated with the considered radiations. Figure 7 shows the estimates of unknown parameters. It is seen that the unknown parameters are continuously adapted to the changing operating conditions.

(b) System response to fast changing temperature. Now, a varying temperature profile, in which the changes are carried out between 25 and 65 °C, is considered. The radiation is kept constant and equal to 1000 W/m². The behavior of the controlled system under this test is shown in Figs. 8 and 9. It is seen in Fig. 8 that the proposed controller well manages the PV power by keeping it at the corresponding maximum value for each temperature (see Fig. 3). Figure 9 shows that the estimates $\hat{\rho}_1$ and $\hat{\rho}_2$ of unknown parameters ρ_1 and ρ_2 are automatically readjusted in order to match the new operating conditions.

Secondly, the proposed MPPT algorithm is tested under load variation, and the result is presented in Fig. 10. For this test, the load resistance is varied from 30 to 4.9 Ω at time $t = 0.2$ s (STC: 1000 W/m², 25 °C). It is observed in Fig. 10
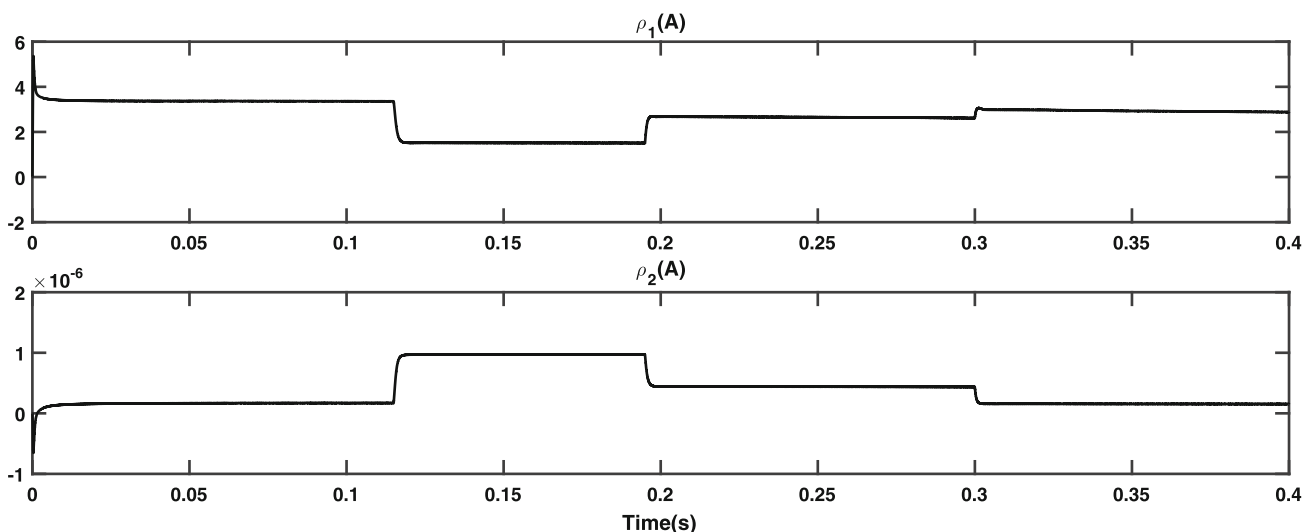
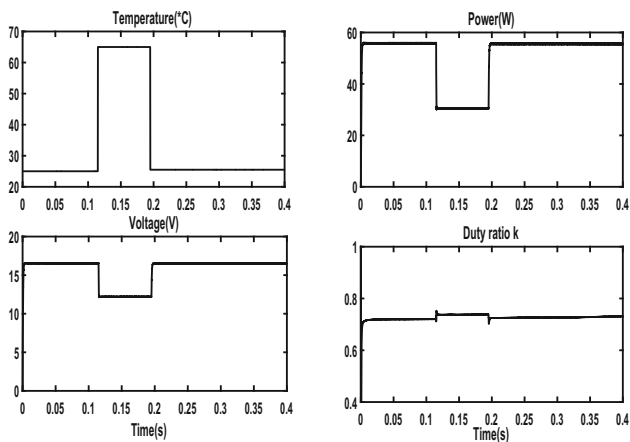**Fig. 7** Estimates of unknown parameters in the presence of radiation variations

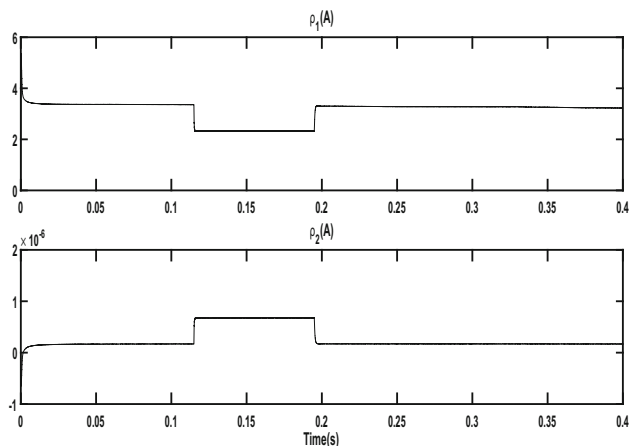**Fig. 8** The proposed MPPT controller during the temperature change

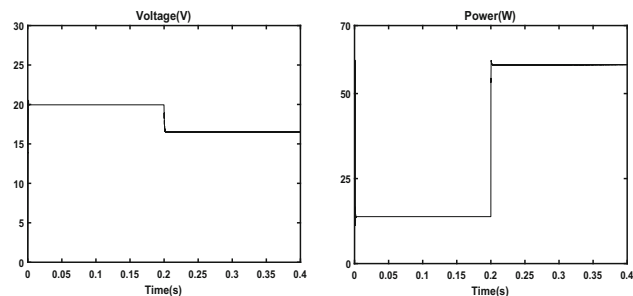**Fig. 9** Estimates of unknown parameters in the presence of temperature variations

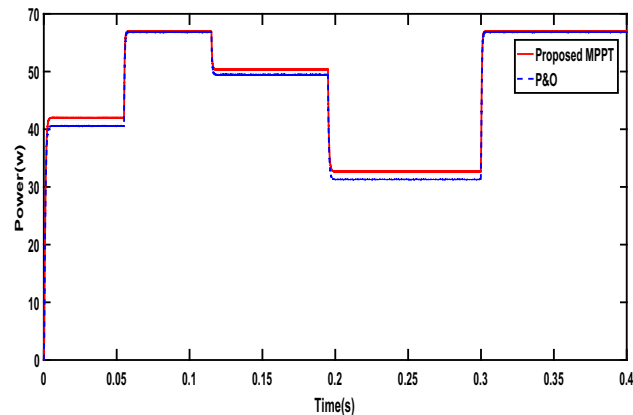**Fig. 10** Load power and load voltage under load variation

Fig. 11 Comparison of the proposed approach with P&O

that the load power increases rapidly from 13.3 to 46 W. Thus, the proposed technique is also able to work under load variation condition.

Finally, a comparative study between the proposed nonlinear neuro-adaptive control approach and the P&O algorithm is established. To have a fair comparison, both algorithms

**Table 2** Qualitative comparison between the proposed method and P&O

MPPT Method	P&O	Proposed MPPT
Power efficiency (η)	0.953	0.97
RMSE	3.3827	2.6596

run under the same conditions. For these test conditions, The power curves for both MPPT algorithms are presented in Fig. 11. It is depicted in this figure that the P&O method presents similar dynamic response compared to that of the proposed method. In contrary, power losses are significant, especially for lower values of irradiation, in the case of P&O method than that of the proposed one. The MPPs obtained in this figure are predictable from the MSX60 characteristics illustrated in Fig. 3. The instantaneous irradiation change imposed on the PV system can be much faster than a real scenario, but gives an idea of how long it takes for the proposed controller to react to an irradiation change. The comparison of quantitative results obtained from Fig. 11 is presented in Table 2. Root mean square error (RMSE) and efficiency are evaluated using the following equations:

$$\text{RMSE} = \sqrt{\frac{\sum (P_{ac} - P_{si})^2}{N}} \qquad (44)$$

$$\eta = \frac{P_{out}}{P_{PV}} \qquad (45)$$

where P_{ac} is the actual value of maximum power obtained from the characteristics as in Table 1. P_{si} is the simulated value of the maximum power for both proposed and P&O techniques; N is the number of samples. The analysis of these results coupled to the fact that temperature and irradiation sensors are not needed clearly demonstrates the superiority of the proposed MPPT algorithm compared to the P&O method.
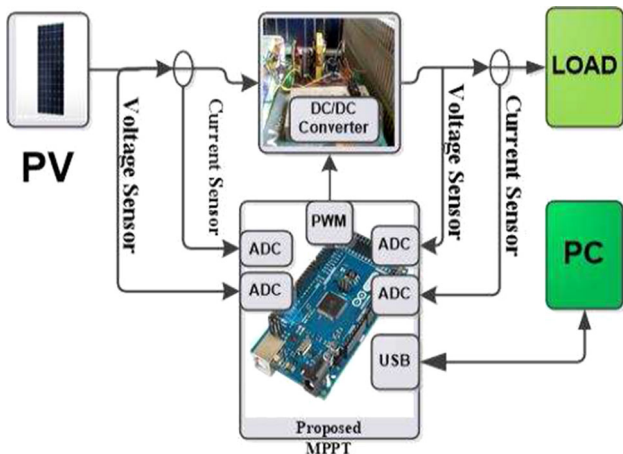
Fig. 12 Experimental architecture
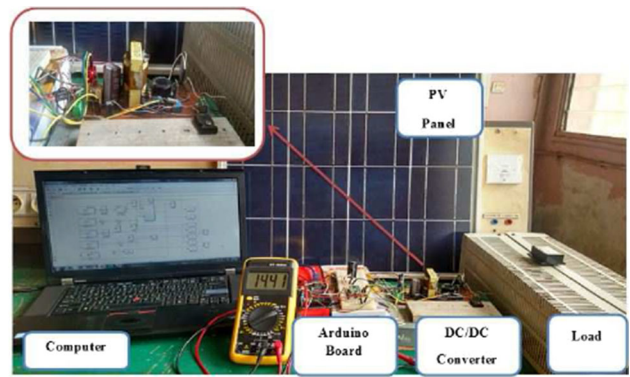
**Fig. 13** Experimental setup for testing and verification of the results
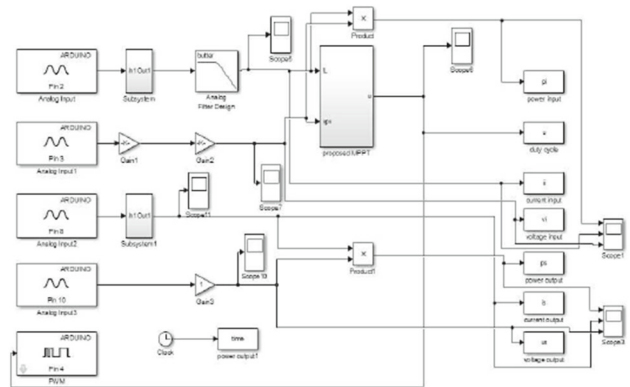
Fig. 14 Experimental design of the proposed algorithm using Arduino under Matlab Simulink

5 Experimental Results

To complete the validation of the proposed MPPT algorithm, experimental system architecture is adopted as shown in Fig. 12. The experimental device, shown in Fig. 13, is constructed using an MSX-60 solar panel, a personal computer, a BOOST DC/DC converter, a resistive load (0–1000 Ω), a control circuit using Arduino Mega board and Hall-effect sensors of ACS 712 type. Two voltage dividers were exploited to obtain the array output voltage and the voltage across the load. An Arduino Mega board is used to execute the proposed MPPT algorithm and deliver the external PWM signal needed to control the BOOST converter. The analog current and voltage values of the solar PV array are fed to the 10-bit ADC module of the Arduino Mega board to be converted into the digital values using current and voltage sensors. The proposed nonlinear adaptive controller was implemented and compiled in the Matlab/Simulink. To control the whole system, the program is downloaded in real time on the Arduino board. The Matlab/Simulink model showing the implementation of the proposed controller using Arduino Mega board is illustrated in Fig. 14.
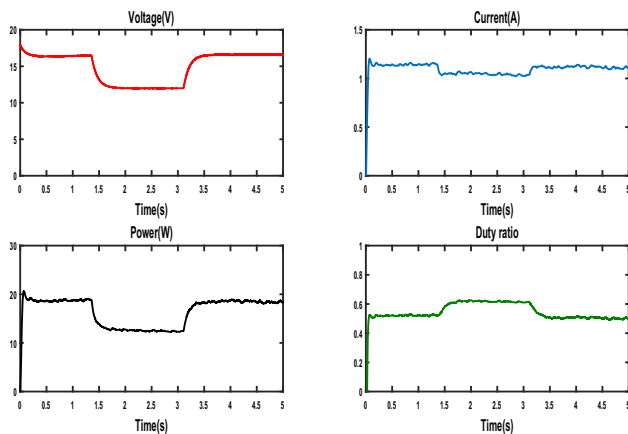
Fig. 15 Experimental results (voltage, current, power and duty ratio) of the proposed MPPT controller

Figure 15 shows the experimental results of the proposed controller. It is observed that the system starts with nearly constant irradiance. During this stable atmospheric conditions, the results confirm the ability of the proposed controller to ensure the stability and the efficiency of the system. At $t = 1.36$ s, the irradiance is abruptly reduced. It is observed that during this sudden change, the proposed controller properly tracks the new maximum power point.

6 Conclusion

In this paper, a new solution to the MPPT issue for PV systems is developed. The MPPT is achieved using an adaptive nonlinear controller based on an artificial neural network approach. The latter takes into account the boost converter nonlinear dynamics. The controller adaptive feature has been introduced to lessen the requirements of temperature and irradiation sensors and also to cope with the changing operating conditions. Simulations have been executed in MATLAB/Simulink environment, and a real-time implementation using Arduino board has been conducted. simulation results were compared to those obtained with the P&O technique. Based on both numerical and experimental results, the proposed control algorithm accurately tracks the maximum power point with a shorter time during abrupt changes in atmospheric conditions.

Compliance with Ethical Standards

References

Ahmed-Ali, T., Kenne, G., & Lamnabhi-Lagarrigue, F. (2009). Identification of nonlinear systems with time-varying parameters using a sliding-neural network observer. *Neurocomputing*, *72*, 1611–1620.

Al-Amoudi, A., & Zhang, L. (2000). Application of radial basis function networks for solar-array modelling and maximum power-point prediction. *IEE Proceedings-Generation, Transmission and Distribution*, *147*(5), 310–316.

Baek, J. W., Ko, J. S., Choi, J.-S., Kang, S. J., & Chung, D. H. (2010). Maximum power point tracking control of photovoltaic system using neural network. In *International conference on electrical machines and systems (ICEMS)* (pp. 638–643).

Bekker, B., & Beukes, H. J. (2004). Finding an optimal PV panel maximum power point tracking method. In *Proceedings of the 7th AFRICON conference Africa* (pp. 1125–1129).

Bendib, B., Krim, F., Belmili, H., Almi, M. F.,& Bolouma, S. (2014). An intelligent MPPT approach based on neural-network voltage estimator and fuzzy controller, applied to a stand-alone PV system. In *IEEE 23rd international symposium on industrial electronics (ISIE)* (pp. 404–409).

Cha, I. S., Choi, J. G., Yu, G. J., Jung, M. W., Baek, H. L., & Kim, D. H. (1997). MPPT for temperature compensation of photovoltaic system with neural networks. In *Photovoltaic specialists conference record of the 26th IEEE* (pp. 1321–1324).

Chen, W., Duan, Y., Guo, L., Xuan, Y., & Yang, X. (2016). Modeling and prediction of radiated emission from solar cell in a photovoltaic generation system. *IEEE Journal of Photovoltaics*, *6*, 540–545.

Femia, N., Petrone, G., Spagnuolo, G., & Vitelli, M. (2005). Optimization of perturb and observe maximum power point tracking method. *IEEE Transactions on Industrial Electronics*, *20*(4), 73–963.

Femia, N., Petrone, G., Spagnuolo, G., & Vitelli, M. (2009). A technique for improving P&O MPPT performances of double-stage grid-connected photovoltaic systems. *IEEE Transactions on Industrial Electronics*, *56*, 4473–82.

Giraud, F., & Salameh, Z. M. (1999). Analysis of the effects of a passing cloud on a grid-interactive photovoltaic system with battery storage using neural networks. *IEEE Transactions on Energy Conversion*, *14*(4), 1572–1577.

Hiyama, T., Kouzuma, S., & Imakubo, T. (1995). Identification of optimal operating point of PV modules using neural network for real time maximum power tracking control. *IEEE Transactions on Energy Conversion*, *10*(2), 360–7.

Jain, A. K., & Dubes, R. C. (1988). *Algorithms for clustering data*. Prentice-Hall: Englewood Cliffs.

Kamarzaman, N. A., & Tan, C. W. (2013). A comprehensive review of maximum power point tracking algorithms for photovoltaic systems. *Renew Sustain Energy*, *37*, 98–585.

Kenne, G., Douanla, R. M., & Pelap, F. B. (2017). An adaptive nonlinear control strategy for a stand-alone permanent magnet synchronous generator driven by a variable speed wind turbine. *International Journal of Dynamics and Control*, *5*, 1103–1113.

Ko, J. S., Jung, B. J., Park, K. T., Choi, C. H. & Chung, D. H. (2008). Maximum power point tracking control of PV system for DC motors drive with neural network. In *International conference on smart manufacturing application. ICSMA* (pp. 514–519).

Kobayashi, K., Matsuo, H., & Sekine, Y. (2004). A novel optimum operating point tracker of the solar cell power supply system. In *Proceedings of the 35th annual power electronics specialists conference* (pp. 2147–2151).

Krein, P. T., Bentsman, J., Bass, R. M., & Lesieutre, B. (1990). On the use of averaging for analysis of power electronic system. *IEEE Transactions on Power Electronics*, *5*(2), 182–190.

Kwon, J., Kwon, B., & Nam, K. (2008). Three-phase photovoltaic system with three level boosting MPPT control. *IEEE Transactions on Power Electronics*, 23, 2319–2327.

Larbes, C., Cheikh, S., Obeidi, T., & Zerguerras, A. (2009). Genetic algorithms optimized fuzzy logic control for the maximum power point tracking in photovoltaic system. *Renewable Energy*, 34(10), 2093–100.

Le Feuvre, M., & Wieczorek, M. A. (2011). Nonuniform cratering of the Moon and a revised crater chronology of the inner solar system. *Icarus*, 214, 1–20.

Li, G., & Wang, H. A. (2009). Novel stand-alone PV generation system based on variable step size INC MPPT and SVPWM control. In *Proceedings of the IEEE 6th international power electronics and motion control conference, IEEE-IPEMC. 09* (pp. 2155–2160).

Liu, F., Kang, Y., Zhang, Y., & Duan, S. (2008). Comparison of P&O and hill climbing MPPT methods for grid-connected PV converter. In *Proceedings of the 3rd IEEE conference on industrial electronics and applications, (ICIEA)* (pp. 804–807).

Masters, G. (2004). *Renewable and efficient electric power systems*. Hoboken: Wiley.

Mathew, A., & Selvakumar, A. I. (2011). MPPT based stand-alone water pumping system. In *2011 international conference on computer, communication and electrical technology (ICCCET)* (pp. 455–460). IEEE.

Mills, A. D., & Wiser, R. H. (2013). Changes in the economic value of photovoltaic generation at high penetration levels: A pilot casestudy of California. *IEEE Journal of Photovoltaics*, 3(4), 1394–1402.

Moura, S. J., & Chang, Y. A. (2013). Lyapunov-based switched extremum seeking for photovoltaic power maximization. *Control Engineering Practice*, 21, 971–80.

Mutoh, N., Matuo, V., Okada, K., & Sakai, M. (2002). Prediction-databased maximum-power-pointtracking method for photovoltaic power generation systems. In *Proceedings of the IEEE 33rd annual power electronics specialists conference* (pp. 1489–1494).

Pachauri, R. K., & Chauhan, Y. K. (2014). Hydrogen generation/pressure enhancement using FC and ANN based MPPT assisted PV system. In *Innovative applications of computational intelligence on power, energy and controls with their impact on humanity (CIPECH)* (pp. 427–432).

Parra, D., Gillott, M., Norman, S. A., & Walker, G. S. (2015). Optimum community energy storage system for PV energy time-shift. *Applied Energy*, 137, 576–587.

Rajabi, M. S., & Hassan Hosseini, M. (2019). Maximum power point tracking in photovoltaic systems under different operational conditions by using ZA-INC algorithm. *SN Applied Sciences*, 2, 1535.

Reisi, A. R., Moradi, M. H., & Jamasb, S. (2013). Classification and comparison of maximum power point tracking techniques for photovoltaic system: A review. *Renewable and Sustainable Energy Reviews*, 19, 433–43.

Rekioua, D., & Matagne, E. (2012). *Optimization of photovoltaic power systems: Modelization, simulation and control*. London: Springer.

Rezaei, M. M., & Asadi, H. (2005). Modified perturb-and-observe-based maximum power point tracking technique for photovoltaic energy conversion systems. *Journal of Control, Automation and Electrical Systems*, 30, 822–831.

Safari, A., & Mekhilef, S. (2011). Simulation and hardware implementation of incremental conductance MPPT with direct control method using cuk converter. *IEEE Transactions on Industrial Electronics*, 58(4), 1154–61.

Sajadian, S., & Ahmadi, R. (2017). Distributed maximum power point tracking using model predictive control for photovoltaic energy harvesting architectures based on cascaded power optimizers. *IEEE Journal of Photovoltaics*, 7, 849–857.

Singh, M. D., Shine, V. J., & Janamala, V. (2014). Application of artificial neural networks in optimizing MPPT control for standalone solar PV system. In *2014 international conference on contemporary computing and informatics (IC3I)* (pp. 162–166).

Slotin, J. J., & Li, W. (1991). *Applied Nonlinear Control*. New York: Prentice-Hall.

Tan, Y. T., Kirschen, D. S., & Jenkins, N. (2010). A model of PV generation suitable for stability analysis. *IEEE Transactions on Energy Conversion*, 19(4), 748–755.

Tchouani Njomo, A. F., Kenne, G., Douanla, R. M., & Sonfack, L. L. (2020). A modified ESC algorithm for MPPT applied to a photovoltaic system under varying environmental conditions. *International Journal of Photoenergy*, 2020, 1–15.

Vachtsevanos, G., & Kalaitzakis, K. (1987). A hybrid photovoltaic simulator for utility interactive studies. *IEEE Transactions on Energy Conversion*, 2, 227–231.

Veerachary, M., Senjyu, T., & Uezato, K. (2003). Neural-network-based maximum-powerpoint tracking of coupled-inductor interleaved-boost-converter-supplied PV system using fuzzy controller. *IEEE Transactions on Industrial Electronics*, 50(4), 749–758.

Villalva, M. G., Gazoli, J. R., & Filho, E. R. (2009). Comprehensive approach to modeling and simulation of photovoltaic arrays. *IEEE Transactions on Power Electronics*, 24(5), 1198–1208.

Won, C. Y., Kim, D. H., Kim, S. C., Kim, W. S., & Kim, H. S. (1994). A new maximum power point tracker of photovoltaic arrays using fuzzy controller. In *Proceedings of the 25th annual IEEE power electronics specialist conference* (pp. 396–403).

Yin, C., Chen, Y. Q., Stark, B., & Zhong, S. M. (2015). Extremum seeking control with fractional-order switching technique design for maximum power point tracking in photovoltaic systems. In *54th IEEE conference on decision and control (CDC)* (pp. 5629–5634).

Yuvarajan, S., & Xuc, S. (2003). Photo-voltaic power converter with a simple maximum-powerpoint-tracker. In *Proceedings of the international symposium on circuits system* (pp. III–399–III-402).